



HHS Public Access

Author manuscript

Inorg Chem. Author manuscript; available in PMC 2024 July 10.

Published in final edited form as:

Inorg Chem. 2023 July 10; 62(27): 10592–10604. doi:10.1021/acs.inorgchem.3c00794.

An ATCUN-like copper site in β B2-crystallin plays a protective role in cataract-associated aggregation

Martin E. Tovar-Ramírez¹, Nils Schuth¹, Oscar Rodríguez², Thomas Kroll³, Gloria Saab-Rincon⁴, Miguel Costas², Kirsten Lampi⁵, Liliana Quintanar^{1,*}

¹Department of Chemistry, Centro de Investigación y de Estudios Avanzados (Cinvestav), Mexico City, 07360, Mexico.

²Facultad de Química, Universidad Nacional Autónoma de México (UNAM), Mexico City, 04510, Mexico.

³Stanford Synchrotron Radiation Lightsource (SSRL), SLAC National Accelerator Laboratory, Menlo Park, 94025, CA, USA

⁴Department of Biocatalysis and Cellular Engineering, Instituto de Biotecnología, Universidad Nacional Autónoma de México, Cuernavaca, Morelos, 62210, Mexico.

⁵Integrative Biosciences, Oregon Health & Science University, Portland, Oregon, 97239, United States.

Abstract

Cataracts is the leading cause of blindness worldwide and it is caused by crystallin damage and aggregation. Senile cataractous lenses have relatively high levels of metals, while some metal ions can directly induce aggregation of human γ -crystallins. Here we evaluated the impact of divalent metal ions in the aggregation of human β B2-crystallin, one of the most abundant crystallins in the lens. Turbidity assays showed that Pb^{2+} , Hg^{2+} , Cu^{2+} , and Zn^{2+} ions induce the aggregation of β B2-crystallin. Metal-induced aggregation is partially reverted by a chelating agent, indicating formation of metal-bridged species. Our study focused on the mechanism of copper-induced aggregation of β B2-crystallin, finding that it involves metal-bridging, disulfide-bridging, and loss of protein stability. Circular dichroism (CD) and electron paramagnetic resonance (EPR) revealed the presence of at least three Cu^{2+} binding sites in β B2-crystallin; one of them with spectroscopic

*Corresponding Author: Liliana Quintanar, Department of Chemistry, Cinvestav. lilianaq@cinvestav.mx.

Author Contributions

The manuscript was written through contributions of all authors. All authors have given approval to the final version of the manuscript.

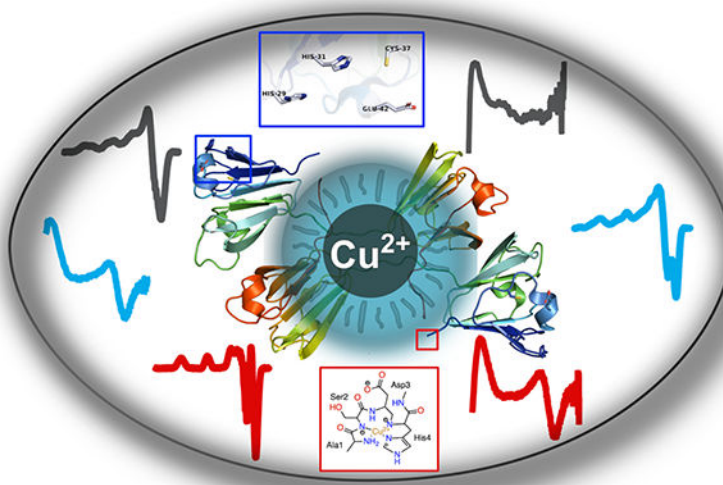
ASSOCIATED CONTENT

Supporting Information

Sequence alignment of human β B2-crystallin with the more abundant γ - and β -crystallins. SDS-PAGE analysis of the β B2-crystallin aggregates with various metal ions. Time dependent effect of EDTA in the copper induced aggregation of β B2-crystallin. Effect of different reducing agents in the β B2-crystallin aggregates, as analyzed by SDS-PAGE. Comparison of EPR and CD spectra of copper-bound β B2-crystallin and HSA. Raw ITC data and their integration of β B2-crystallin and the β B2-peptide. Titration of the N-truncated protein with copper ions as followed by circular dichroism. SDS-PAGE analysis of Cu-induced aggregates of N-truncated β B2-crystallin. Chromatogram and Mass spectrometry analysis of the peptide β B2(1–6) ASDHQF. Size exclusion chromatograms of WT and N-truncated β B2-crystallins. SDS-PAGE purity analysis of both proteins. All thermal denaturation traces. Comparison of EPR spectra for β B2- and γ D- crystallins with copper. Copper EPR simulations parameters for the ATCUN-like site in β B2-crystallin. Thermodynamic parameters for the Gibbs-Helmholtz fit of the thermal denaturation experiments with β B2-crystallin WT and the N-truncated protein. And full chromatography reports. The Supporting Information is available free of charge on the ACS Publications website.

features typical of Cu^{2+} bound to an amino-terminal copper and nickel binding motif (ATCUN), a motif found in Cu transport proteins. The ATCUN-like Cu binding site is located at the unstructured N-terminus of βB2 -crystallin, and it could be modeled by a peptide with the first six residues in the protein sequence ($\text{NH}_2\text{-ASDHQF-}$). Isothermal titration calorimetry indicates a nanomolar Cu^{2+} binding affinity for the ATCUN-like site. Removal of the N-terminus yields an N-truncated form of βB2 -crystallin that is more susceptible to Cu-induced aggregation and loss of thermal stability, indicating a protective role for the ATCUN-like site. EPR and X-ray absorption spectroscopy (XAS) studies reveal the presence of a copper redox active site in βB2 -crystallin that is associated to metal-induced aggregation and formation of disulfide-bridged oligomers. Our study demonstrates metal-induced aggregation of cataract-related βB2 -crystallin and the presence of putative copper binding sites in the protein. Whether the copper-transport ATCUN-like site in βB2 -crystallin plays a functional/protective role or constitute a vestige from its evolution as a lens structural protein, remains to be elucidated.

Graphical Abstract



Keywords

Metal ions; beta-crystallins; copper; ATCUN site; metal-induced aggregation; cataract disease

Introduction

Cataract disease is the leading cause of blindness worldwide, and it is associated with an opacification of the eye lens, due to the formation of high-molecular-weight protein aggregates that scatter light and interfere with the vision process.¹ Crystallins are the most abundant proteins in the eye lens, constituting around 90% of its soluble protein content, and reaching concentrations of ~ 600 mg/ml.^{2, 3} Crystallins are classified into two families: α -crystallins and $\beta\gamma$ -crystallins.^{4, 5} α -crystallins form large protein oligomers with chaperone-like activity, that can recognize and bind damaged and partially unfolded proteins to keep them soluble.⁶ On the other hand, $\beta\gamma$ -crystallins are smaller structural and refractive

proteins, and in turn are divided into: γ -crystallins, which can be found in a monomeric state; and β -crystallins, which usually form dimers and oligomers.^{3, 4} β B2-crystallin is one of the most abundant β -crystallins, and it constitutes 14% of the total protein content of a young lens.^{3, 7} This protein has been associated with congenital cataracts, specifically the A2V mutation of the protein.^{8, 9} Although the role of β B2-crystallin in the eye lens is mainly a structural one, various reports have found that the CRYBB2 gene is not only expressed in the eye lens, but also in the retina, brain, and testis, suggesting that this protein may have different functions other than a refractive one.^{10–12} Some members of the $\beta\gamma$ -crystallin family, such as bacterial protein S, fungal spherulin 3a and Ci- $\beta\gamma$ -crystallin in the urochordate *Ciona intestinalis*, bind Ca^{2+} ions to stabilize their structure and they may be implicated in calcium signaling.^{13–16} Some evidence suggests that the latter, Ci- $\beta\gamma$ -crystallin, may coordinate to other divalent metal cations such as Mg^{2+} , Co^{2+} , Zn^{2+} , Sr^{2+} , Mn^{2+} , Ni^{2+} .¹⁷ The human β B2-crystallin can also coordinate Ca^{2+} ions *in vitro*, a finding that suggests a possible physiological role for human β B2-crystallins in calcium dependent processes.¹⁸

Senile cataractous lenses contain higher levels of metals, such as copper and zinc, as compared with healthy lenses,^{19–26} suggesting a potential role of metal ions in the etiology of cataract disease. Indeed, recent studies have shown that Cu^{2+} and Zn^{2+} ions induce non-amyloid aggregation of the three most abundant γ -crystallins in the human lens.^{17, 27–31}

Specifically, Zn^{2+} ions induce the aggregation of human γ D-crystallin by a mechanism that involves exclusively the formation of metal-bridged species,²⁷ while Cu^{2+} ions induce γ -crystallin aggregation by several different mechanisms, including metal-induced unfolding of the protein, copper redox activity, and formation of metal-bridged and disulfide-bridged species.^{28, 31} Some putative metal binding sites involved in metal-induced aggregation have been identified in γ -crystallins. While β -crystallins do not display the same metal binding motifs as γ -crystallins, they share some similarities in regions containing putative metal anchoring residues (Figure S1). Still, the susceptibility of β -crystallins towards metal-induced aggregation has not been tested.

In this study, we expand our knowledge of the bioinorganic chemistry of cataract disease, evaluating the impact of metal ions in the aggregation of β B2-crystallin, one the most abundant β -crystallins in the human lens. Our study focuses on the mechanism of copper-induced aggregation of β B2-crystallin, and the elucidation of its copper binding properties. Spectroscopic analysis using circular dichroism (CD), electron paramagnetic resonance (EPR) and X-ray absorption and emission spectroscopy (XAS/XES) reveals unique and interesting putative copper binding sites in human β B2-crystallin.

Results

1. Metal-induced aggregation of β B2-crystallin.

The impact of different metal ions in the aggregation of β B2-crystallin was evaluated by turbidity assays. Different divalent metal ions (Mn^{2+} , Ca^{2+} , Ni^{2+} , Hg^{2+} , Pb^{2+} , Zn^{2+} , Cu^{2+}) were added to the protein solution, and their effect on protein aggregation was measured by turbidity at 400 nm (Fig. 1a). Mercury, lead, zinc, and copper ions induced a drastic

increase in turbidity, reflecting aggregation of the protein, while the addition of manganese, calcium, and nickel ions had no effect. The effect of adding an excess (100 equiv) of a chelating agent, ethylenediaminetetraacetic acid (EDTA), on metal-induced aggregation was evaluated (Fig. 1B); in all cases, a significant decrease in turbidity was observed. The effect of EDTA on the zinc-induced aggregation of β B2-crystallin is of particular interest, as it can completely reverse the turbidity, in a similar fashion as previously observed for the zinc-induced aggregation of human γ D crystallin,²⁷ suggesting that metal-bridging may be the prominent mechanism for zinc-induced aggregation of β B2-crystallin. Moreover, SDS-PAGE analysis of the metal-induced aggregates reveal that, upon treatment with both, EDTA and a reducing agent such as 2-mercaptoethanol (BME), the metal-induced aggregates can be disaggregated into protein monomers (Figure S2). Overall, these results suggest that metal-induced aggregation of β B2-crystallin involves, at least to some extent, a metal-bridging mechanism. In the present study, the mechanisms involved in Cu-induced aggregation will be examined.

2. Copper-induced aggregation of β B2-crystallin.

The effect of adding different equivalents of Cu^{2+} ions in the aggregation of β B2-crystallin was examined by turbidity assays (Fig. 2, A & B). While the addition of 1 equivalent of Cu^{2+} had no effect in the aggregation of β B2-crystallin, higher amounts of the metal ion caused a drastic increase in turbidity, reaching a maximum effect at > 4 equiv. Interestingly, the addition of 100 equivalents of EDTA fully reversed the turbidity at < 4 equivalents of Cu^{2+} ions, while with higher Cu:protein ratios, the chelating agent can only partially reduce the turbidity (Fig 2B). Hence, the chelating agent is less able to revert the turbidity, as the copper concentration increases. Moreover, the ability of EDTA to revert Cu-induced aggregation decreases as the time of exposure to the metal increases (Figure S3). These results suggest that there are other mechanisms involved in Cu-induced aggregation of β B2-crystallin, beyond metal bridging.

Protein aggregates at the endpoint of the turbidity assays were separated by centrifugation and analyzed by SDS-PAGE (Fig 2, C & D). In all cases, a band that corresponds to a monomeric species is observed, except for the sample with 1 equivalent of Cu, suggesting that an equimolar concentration of the metal ion is not enough to promote protein aggregation. A second band can be seen just below the protein monomer (Fig 2C), possibly due to the formation of an intramolecular disulfide bond, as the addition of 2-mercaptoethanol (BME) results in disappearance of this band (Fig 2D). For protein aggregates formed in the absence of a chelating agent, SDS-PAGE analysis without a reducing agent shows the presence of a dimeric species at > 2 equiv of Cu, while several bands at higher molecular weight are readily seen at > 5 equiv, indicating the presence of various oligomerization states of the protein (Fig 2C). These bands grow in intensity as the copper concentration increases, suggesting that the aggregation mechanism depends on metal ion concentration. The addition of EDTA reduces drastically the abundance of these higher molecular weight species in the aggregate (Fig. 2C), while they completely disappear when the SDS-PAGE analysis is performed in the presence of BME (Fig. 2D). The use of other reducing agents, such as tris(2-carboxyethyl) phosphine (TCEP) or dithiothreitol (DTT), also cause high molecular weight species to disappear (Figure

S4). SDS-PAGE analysis under reducing conditions of Cu-induced aggregates formed in the presence of EDTA display mostly a monomeric species. These results suggest that Cu-induced aggregates of β B2-crystallin are formed mostly through metal-bridging and disulfide-bridging interactions, although further studies would be needed to confirm the presence of disulfide bridges in the aggregates.

3. Copper coordination to β B2-crystallin.

The nature of Cu^{2+} binding by β B2-crystallin was investigated by titrating the protein with 0 to 4 equivalents of metal ion, followed by circular dichroism (CD) and electron paramagnetic resonance (EPR) (Fig. 3). EPR spectra show three spectroscopic features that correspond to at least three Cu^{2+} binding modes (Fig. 3A). All EPR signals display g_{\parallel} factor $> g_{\perp}$ indicating a $d_{x^2-y^2}$ ground state for all Cu^{2+} species. From 0.5 to 2 equiv of metal ion, two main species are observed, the most abundant one displays a $g_{\parallel}=2.204$ and ${}^{\text{Cu}}A_{\parallel}=210 \times 10^{-4} \text{ cm}^{-1}$ and will be referred to as Mode 1. The second spectroscopic species has a $g_{\parallel}=2.260$ and ${}^{\text{Cu}}A_{\parallel}=198 \times 10^{-4} \text{ cm}^{-1}$ and is termed Mode 2. When more than 2 equivalents Cu^{2+} are added, a third set of signals appears with $g_{\parallel}=2.290$ and ${}^{\text{Cu}}A_{\parallel}=181 \times 10^{-4} \text{ cm}^{-1}$, and it grows between 2 and 4 equiv of metal ion without apparent saturation. These results clearly show that there are at least three Cu^{2+} binding sites in β B2-crystallin.

A titration of β B2-crystallin followed by CD shows that upon addition of the first equivalent of Cu^{2+} , the growth of a negative signal at $17,270 \text{ cm}^{-1}$, a small positive one at $20,700 \text{ cm}^{-1}$ and another positive one at $32,575 \text{ cm}^{-1}$ is observed (Fig. 3B); the first two are ligand field transitions (d-d bands), while the latter one is a ligand to metal charge transfer (LMCT) band that could be assigned to a deprotonated amide to Cu^{2+} transition, although the contribution from a LMCT from imidazole π^1 to Cu^{2+} cannot be discarded.^{32–37} Upon addition of more metal ion, the negative d-d band and the LMCT band increase in intensity reaching a maximum at 3 equivalents, while the positive d-d band disappears and a shoulder to the LMCT band appears at $29,800 \text{ cm}^{-1}$; the latter can be assigned as a LMCT from imidazole π^1 to Cu^{2+} . Overall, the CD data are consistent with having three Cu^{2+} binding sites in β B2-crystallin involving imidazole residues, while the highest affinity site (Mode 1) also involves the contribution of deprotonated amides or imidazole from a histidine or both.

The spectroscopic features of the first Cu^{2+} binding site (Mode 1) in β B2-crystallin resemble those of a copper ion bound to an amino-terminal Copper/Nickel (ATCUN) binding motif present in peptides and proteins involved in copper trafficking, such as human serum albumin (HSA).^{38–42} Indeed, a comparison of the CD and EPR spectra of Cu^{2+} bound to β B2-crystallin with those of Cu^{2+} bound to HSA reveals striking similarities (Fig. S5), strongly suggesting the presence of an ATCUN motif in this crystallin. ATCUN sites include a free N-terminal group and a His residue in the third position of the sequence, yielding highly stable complexes with Cu^{2+} .^{43–46} In the case of β B2-crystallin, it has a His residue in the fourth position at the N-terminal, with sequence $\text{NH}_2\text{-ASDH-}$ (Fig. S1). While this is technically not a canonical ATCUN motif, the proximity of His4 to the free NH_2 group could allow for an effective anchoring for Cu^{2+} , yielding a complex that is very similar to that found in HSA. Indeed, ATCUN-like sequences have been reported for some copper binding proteins.⁴⁷

To probe if the ATCUN-like spectroscopic features of β B2-crystallin arise from its N-terminal sequence, a peptide with the first six amino acids (NH₂-ASDHQF-) was synthesized as a model. A titration of the peptide β B2(1–6) with Cu²⁺ shows only one set of signals that correspond to $g_{\parallel}=2.206$ and $^{Cu}A_{\parallel}=207 \times 10^{-4} \text{ cm}^{-1}$ (Fig 4A). The signals observed in the EPR spectrum of the peptide-copper complex are identical to those of the main species (Mode 1) in the spectrum of Cu²⁺- β B2-crystallin. Consistently, the CD spectrum of 0.25 equivalents of Cu²⁺ bound to the β B2(1–6) peptide displays a negative d-d band at 17,330 cm⁻¹, a positive one at 20,445 cm⁻¹ and a LMCT band at 32,340 cm⁻¹, and it is almost identical to the CD spectrum of β B2-crystallin with 0.5 equivalents of metal ions (Fig. 6B). Overall, these results demonstrate that the highest affinity binding site for Cu²⁺, termed Mode 1, corresponds to the metal ion bound to the N-terminal sequence of the protein, as modeled by the peptide β B2(1–6). The simulation of the EPR spectrum of the Cu²⁺-peptide complex agrees with spin Hamiltonian values with a 4N coordination mode with four non-equivalent nitrogen donors (Fig 4B, Table S1). This would be consistent with Cu²⁺ bound to the amino group, an imidazole and two deprotonated amides, as proposed for ATCUN-like sites; indeed, the EPR parameters of this complex resemble those of previously reported ATCUN sites.^{38, 40, 41, 43–47}

The copper binding properties of β B2-crystallin WT and the β B2(1–6) peptide were also evaluated by isothermal titration calorimetry (ITC). As shown in Figure 5, the interaction of Cu²⁺ ions with the protein and the peptide are very similar, and the data can be fitted to a stoichiometric equilibria (SE) model, yielding K_d values in the order of nanomolar affinity for both systems: K_d = 0.9 nM for the protein and K_d = 8.5 nM for the peptide (Table 1). It should be noted that ΔH is similar in both systems, and that the low interaction energy and the protein aggregation phenomenon hinder the analysis, so further characterization would be necessary to discriminate other potential binding models that could describe the interaction. Still, the high Cu²⁺ binding affinity (K_d in the nanomolar range) determined for both, the protein and the peptide, is consistent with its identification of an ATCUN-like site with a NH₂-XXXH motif at the N-terminal of this lens protein.

To further characterize the other two Cu²⁺ binding sites in β B2-crystallin (Mode 2 and 3, Fig 3A), an N-truncated version of the protein was prepared, lacking the first eight residues of the sequence. A titration of the N-truncated β B2-crystallin with Cu²⁺ ions, as followed by EPR, shows at least three sets of signals (Fig 6A), none of which correspond to the ATCUN-like site or Mode 1. Interestingly, upon addition of the first two equivalents of metal ion, two species are observed: one with $g_{\parallel}=2.262$ and $^{Cu}A_{\parallel}=186 \times 10^{-4} \text{ cm}^{-1}$ that corresponds to Mode 2; and a new species with $g_{\parallel}=2.235$ and $^{Cu}A_{\parallel}=167 \times 10^{-4} \text{ cm}^{-1}$, that is termed Mode 4 (Fig 6A). When more than two equivalents of Cu²⁺ are added, a third set of signals appears with $g_{\parallel}=2.285$ and $^{Cu}A_{\parallel}=181 \times 10^{-4} \text{ cm}^{-1}$, that correspond to the Mode 3 observed in the wild type (WT) protein.

The interaction of the N-truncated protein with Cu²⁺ ions was also evaluated by CD, showing predominantly a positive band at 31,575 cm⁻¹ (Fig 6B) that can be assigned to a LMCT from an imidazole π^1 to Cu²⁺, and saturates at one equivalent of copper. This signal differs from those observed in the spectra of β B2-crystallin WT and the β B2(1–6) peptide, and it may be associated to Mode 2, which would explain the broadening observed at higher

equivalents of metal ion in the titration of the WT protein (Fig 3A). It also suggests that Mode 2 involves histidine binding. The characteristic CD signals of the ATCUN-like site (Mode 1) were not observed (Fig. 6B). Further titration of the N-truncated protein with Cu^{2+} results in the formation of a positive signal at approximately $26,000\text{ cm}^{-1}$ and a negative around $21,000\text{ cm}^{-1}$. The truncation leads to drastic protein aggregation that prevented collection of CD data with adequate signal to noise ratio (Fig. S7).

In summary, the truncation of the N-terminal residues of βB2 -crystallin effectively removes the ATCUN-like Cu^{2+} binding site, while the presence of Mode 2 and 3 remain with similar EPR features as observed in the full protein. Unfortunately, the unexpected appearance of mode 4 and a drastic copper induced aggregation of the N-truncated protein complicate the spectroscopic analysis of the metal binding sites. Furthermore, the fact that the signals associated to Mode 4 are not observed for the WT protein suggests that this fourth site may become accessible after truncation of the protein.

4. A redox active site in βB2 -crystallin.

A previous study of γ -crystallins shows that Cu^{2+} coordination to these proteins can lead to reduction of the metal ion under aerobic conditions.⁴⁹ Here we have used EPR and X-ray absorption/emission spectroscopy (XAS/XES) to probe if the Cu^{2+} binding sites in βB2 -crystallin are redox-active (Fig. 7). These experiments were performed with one equiv of Cu^{2+} ions; under these conditions Mode 1 and Mode 2 are observed for the βB2 -crystallin WT, while Mode 2 is predominantly observed for the N-truncated protein by EPR (Fig. 7A). Spin quantitation of these spectra account for $\sim 60\%$ of the Cu^{2+} ions added to βB2 -crystallin WT and for $\sim 70\%$ in the case of the N-truncated protein, suggesting the possibility that some of the Cu^{2+} ions are reduced to Cu^+ . Indeed, XANES spectra of these samples show the distinct K-edge feature below $8,985\text{ eV}$ characteristic for low-coordinated (linear or trigonal) Cu^+ species, and corresponds to a $1s \rightarrow 4p$ electronic transition (Fig 7B).⁵⁰ These results clearly demonstrate the presence of Cu^+ ions bound to βB2 -crystallin WT and its N-truncated form. It is important to note that this Cu^+ spectroscopic feature is not observed in the Cu - $\beta\text{B2}(1-6)$ sample (Fig 7B), strongly suggesting that the redox active site in the protein does not correspond to the ATCUN-like site. Moreover, normalized XES spectra showing $2p \rightarrow 1s$ transitions for Cu^+ bound to βB2 -crystallin WT and its N-truncated form are identical (Fig 7C), suggesting that these two proteins display the same Cu^+ binding site, and further confirming that Cu^+ binding does not involve the N-terminal region of the protein.

XANES spectra also show weak absorptions between $8,975 - 8,980\text{ eV}$, corresponding to $1s \rightarrow 3d$ transitions of Cu^{2+} species (Fig. 7B, inset). Clearly, the Cu^{2+} signal of the N-truncated protein is shifted to lower energy, as compared to those for βB2 -crystallin WT and the peptide. This reflects a stronger ligand-field for the latter Cu^{2+} species, consistent with the presence of an ATCUN-like complex in both, the WT-protein, and the peptide. Likewise, XES spectra show that the $\text{K}\alpha$ emission for Cu^{2+} bound to βB2 -WT and the peptide are quite similar among them, while that of the N-truncated protein shifts to lower energy (Fig. 7D), consistent with a lower ligand-field for Cu^{2+} bound to this variant. Overall,

EPR and XAS studies reveal the presence of a copper redox active site in β B2-crystallin that does not involve its N-terminal ATCUN-like site.

5. N-truncation of β B2-crystallin increases its susceptibility to copper.

The impact of N-truncation in the copper induced aggregation of β B2-crystallin was evaluated. Addition of Cu^{2+} to the N-truncated protein leads to an earlier onset of aggregation as compared to β B2-crystallin WT (Fig. 8 A & B). For the WT protein, an increase in turbidity can be observed only after addition of 2 equivalents of copper ions, whereas for the N-truncated protein, the increase in turbidity can be seen immediately after addition of 1 equivalent of the metal. These results indicate that removal of the high affinity ATCUN-like exacerbates the aggregation induced by copper, suggesting a protective buffering effect for this site. Furthermore, the truncation of the N-terminal peptide does not affect the copper-induced formation of disulfide-bridged oligomers, as shown by SDS-PAGE analysis of the protein aggregates (Fig. S8); suggesting that the ATCUN-like site is not involved in cysteine oxidation. On the other hand, the effect of copper ions in the secondary structure and thermal stability of both proteins was evaluated by CD in the far UV region. For both cases the addition of less than 2 equivalents of copper ions do not cause the reduction of the signal intensity at 218 nm that is characteristic of β -sheet secondary structure, suggesting that copper induces very minor changes on the conformation of the protein at these conditions (Fig. 8 C & D). However, upon addition of the first equivalent of Cu^{2+} ions to β B2-crystallin, a decrease of $\sim 3^\circ\text{C}$ on the melting temperature (T_m) can be observed, as compared to the protein with no copper is added (Fig. 8E).^{8, 51} After addition of the second equivalent of metal ions, a reduction on the T_m of $\sim 6^\circ\text{C}$ can be seen. Remarkably, the N-truncation of the protein makes it more susceptible to thermal denaturation induced by copper: a reduction of $\sim 3^\circ\text{C}$ and $\sim 6^\circ\text{C}$ can be observed as 0.5 and 1 equivalents of the metal are added to the protein solution (Fig. 8F). Altogether, these results suggest that removal of the ATCUN-like site exacerbates copper-induced aggregation and reduction of the thermal stability of β B2-crystallin, as this site may play a protective copper buffering role.

Discussion

In this work we have shown that divalent metal ions, such as Hg^{2+} , Pb^{2+} , Zn^{2+} and Cu^{2+} induce the aggregation of β B2-Crystallin, while Ca^{2+} , Mn^{2+} and Ni^{2+} did not have this effect. It is interesting to note that this correlates with the hard-soft nature of the cations: the latter are the hardest metal ions of the ones tested, while Hg^{2+} and Pb^{2+} are soft metal ions, and Cu^{2+} and Zn^{2+} are intermediate. These results suggest that the coordination site responsible for the aggregation of the protein involves soft ligands such as cysteine and methionine, and hard/soft borderline ligands such as histidine. Indeed, cysteine residues are involved in Hg^{2+} induced aggregation of H γ C and H γ S crystallins,⁵² where formation of disulfide-bridged species have been implicated in the aggregation mechanism. The protein β B2-crystallin has only two cysteines: Cys37 and Cys66, which are likely to participate in Hg^{2+} and Pb^{2+} induced aggregation of β B2-crystallin, possibly forming disulfide-bridged species as in the case of H γ C and H γ S crystallins, but further studies are required to evaluate this hypothesis. In contrast, Zn^{2+} induced aggregation of β B2-crystallin

may involve mostly a metal-bridged mechanism, as it can be fully reverted by addition of EDTA (Fig. 1B). A very similar scenario is observed for Zn^{2+} induced aggregation of $H\gamma D$ crystallin, where His22 in a -CXXXH- motif at the N-terminal domain participates in anchoring the metal ion. While $\beta B2$ -crystallin does not contain such a motif, a multiple sequence alignment of $\beta B2$ -crystallin with $H\gamma D$ (Fig. S1), $H\gamma C$ and $H\gamma S$ crystallins shows the presence of a cysteine residue (Cys37) that prevails at the homologous position of His22; this is also the case for $H\gamma S$ and $H\gamma C$ crystallins. The closest histidine residues to Cys37 in $\beta B2$ -Crystallin are His30 and His32, which are solvent exposed (Fig. 9C), and together with Cys37 could participate in the coordination of Zn^{2+} ions by $\beta B2$ -crystallin.

Copper induced aggregation of $\beta B2$ -crystallin seems to involve several mechanisms including, metal-bridging, disulfide-bridging, loss of protein stability and copper reduction. This complex scenario is partially similar to that observed for copper induced aggregation of human γ -crystallins,⁴⁹ where the mechanism involves: copper coordination, unfolding of the protein, intermolecular oligomerization through disulfide and metal-bridging, and copper redox chemistry that leads to a tyrosine-based radical. No protein-based radical is observed in the case of $\beta B2$ -crystallin (Fig. S14), while all other mechanisms are at work. In the case of γ -crystallins a putative copper binding region has been identified at the N-terminal domain, involving a -CXCXC- motif in γS , and a -CXXXH- motif in γD . Additionally the latter displays a -CXC- motif at the C-terminal domain, that constitutes a putative Cu^+ binding site, like those found in copper chaperone proteins, such as Atox1. In $\beta B2$ -crystallin these putative binding motifs are not present as such, however this protein has a -HXHXXXXXC- motif at the N-terminal domain that is solvent accessible (Fig 9C), where Cys37 is at the homologous position to His22 in the -CXXXH- motif of γD and Cys26 in the -CXCXC- motif of γS . Hence the -HXHXXXXXC- at the N-terminal of $\beta B2$ -crystallin may constitute a putative copper binding site, while the solvent-exposed Cys37 could be engaged in the copper-induced formation of disulfide-bridged oligomers. Indeed, this putative site is likely responsible for metal-induced aggregation and for the observed copper redox activity, since it is the only one involving soft ligands, such as Cys, that can stabilize Cu^+ species as those observed by XAS. Interestingly, Cys37 is also conserved in $\beta A1$, $\beta A3$ and $\beta B1$ crystallins, however the susceptibility of these crystallins towards copper-induced aggregation has not been tested.

Our spectroscopic studies of Cu^{2+} binding to $\beta B2$ -crystallin have revealed the presence of an ATCUN-like site, which displays characteristic EPR and CD spectroscopic features. ATCUN sites are commonly observed in peptides and proteins that bind Cu^{2+} ions with high affinity (K_d in the picomolar range) and are highly conserved in proteins associated with copper transport.^{41, 45, 46} This motif is characterized by having a free amino terminus and a histidine in the third position (H_2N -XXH-), which act as anchoring ligands for Cu^{2+} , while the coordination sphere is completed by a pair of deprotonated amide nitrogens in a square planar fashion (Fig 9A). This coordination geometry is highly stabilized by a chelate effect as it facilitates the formation of two five-membered and one six-membered rings with a Cu^{2+} ion at its center. Interestingly, $\beta B2$ -crystallin possesses a disordered N-terminal region, encompassing 13 amino acids, with a histidine in the fourth position (H_2N -ASDH-), providing an ATCUN-like binding site for copper. Considering that $\beta B2$ -crystallin has the coordinating histidine in the fourth position (Fig. 9A), the chelate stabilization effect may be

decreased, as compared with that of a typical Cu²⁺-ATCUN complex with a histidine in the third position; resulting in a lower metal binding affinity. Indeed, our ITC studies reveal a $K_d = 0.9$ nM for the protein and $K_d = 8.5$ nM for the peptide (Table 1). These values are in the order of other sites with similar motifs, such as the NH₂-AGGH peptide with a $K_d = 0.13$ nM,⁵³ or a model peptide for the human Cu transporter hCtr2 protein with sequence NH₂-MAMHF and a $K_d = 1.1$ nM.⁴⁷ Generally, ATCUN-like sites, with sequences NH₂-XXXH display Cu²⁺ binding affinities that are four to six orders of magnitude lower, as compared to canonical ATCUN sites, such as the NH₂-MDH motif of hCtr1 protein ($K_d = 13$ pM) and the NH₂-FRH motif of the N-terminally truncated amyloid- β peptide (4–40) with $K_d = 30$ fM.⁵⁴ Hence, the Cu²⁺ binding affinity for β B2-crystallin WT and the β B2(1–6) peptide is consistent with its identification of an ATCUN-like site with a NH₂-XXXH motif at the N-terminal of this lens protein.

Consistently, titrations of β B2-crystallin with Cu²⁺ ions indicate that a second binding mode (Mode 2) starts to be populated before the ATCUN-like site (Mode 1) is fully loaded. Still, the latter seems to play a copper buffering role, as removal of the ATCUN-like site exacerbates copper-induced aggregation of β B2-crystallin. Although β B2-crystallin is N-acetylated,⁵⁵ the His in the fourth position could still favor copper binding, as suggested by the Boc-AGGH-Cu(II) complex reported by Pettit et al.⁵³ It is puzzling to find in a lens crystallin protein a Cu binding site and affinity that are typically associated to Cu transport proteins, such as hCtr2.⁴⁷ Interestingly, some studies have proposed that the N-terminal extension of β -crystallins is necessary for protein stability, as the progressive truncation of this region has been associated to cataracts.^{56–59} Particularly, the N-terminal extension of β B2-crystallin becomes ordered due to the formation of hetero tetramers of β B2/ β A3, as it is thought to stabilize the protein complex.⁶⁰ This N-terminal extension suffers from extensive age-related truncation,^{61–63} which in turn can remove the copper binding site and contribute to cataract formation. Whether this ATCUN-like site in β B2-crystallin is a true Cu buffering site, it is required for protein stability, and/or it is a vestige from the evolution of crystallins as lens structural proteins, remains to be elucidated.

Finally, β B2-crystallin EPR spectroscopy reveals the presence of a third Cu²⁺ binding site (Mode 3) with lower affinity that is hard to discern from the other two principal Cu²⁺ coordination sites. However, the EPR parameters associated to Mode 3 are indicative of a 2N2O equatorial coordination mode involved two oxygen-based and two nitrogen-based ligands. Figures 9D and E show plausible Cu binding sites for Mode 3. One is present at the non-structured interdomain connecting loop, containing Asp102, Ser103, Gln104 and His106 (Fig 9D). This sequence is right on the center of the dimer and may coordinate Cu²⁺ with two histidines, one of each protomer, possibly with a concomitant structural change of the loop to accommodate the metal coordination sphere. The other putative site is at a solvent-exposed region of the C-terminal domain, involving Gln137, which is part of a flexible loop, and His132 at a small α -helix motif (Fig 9E). There is also His134 nearby at the beginning of this α -helix, which in principle could be recruited for metal coordination, causing partial unfolding of the helical structure. Together, these two putative copper binding sites would be consistent with the 2N2O coordination sphere found for Mode 3; however, site directed mutagenesis studies would be required to probe these putative metal binding sites.

Conclusions

β B2-crystallin, the most abundant β -crystallin in the human lens, is susceptible to metal-induced aggregation by divalent metal ions, such as Hg^{2+} , Pb^{2+} , Zn^{2+} and Cu^{2+} . Metal-induced aggregation of β B2-crystallin involves the formation of metal-bridged species. While metal-bridging is the main mechanism for zinc-induced aggregation of β B2-crystallin, disulfide-bridging is also involved in the case of mercury, lead and copper.

Our study has focused on the mechanism of copper-induced aggregation of β B2-crystallin, which involves metal-bridging, disulfide-bridging, loss of protein stability and Cu^{2+} reduction to Cu^+ by the protein. Spectroscopic studies reveal the presence of three Cu^{2+} binding sites in β B2 crystallin. Strikingly, one of them is an ATCUN-like Cu binding site located at the unstructured N-terminal region and encompassing the first amino acid residues, namely $\text{NH}_2\text{-ASDHQF-}$. While being a typical Cu^{2+} binding site in copper transport proteins, the ATCUN-like site in β B2-crystallin may play a copper buffering role that protects the protein from metal-induced aggregation in an aging lens. Beyond the N-terminal ATCUN-like site, EPR and XAS studies reveal the presence of a copper redox active site in β B2-crystallin that is likely the site responsible for metal-induced aggregation and formation of disulfide-bridged oligomers. This putative redox-active copper binding site may involve His29, His31, and Cys37 in the -HXHXXXXXC- motif at the N-terminal domain of β B2-crystallin.

While the mechanisms of metal-induced aggregation of β B2-crystallin and the nature of all metal binding sites in this human lens protein requires further investigation, the fact that essential metal ions, such as copper and zinc, can induce the aggregation of one of the most abundant crystallins in the human lens, further supports a role for metal ions in cataract disease. Most interestingly, the presence of canonical Cu^{2+} binding sites, such as the ATCUN-like site in β B2-crystallin is most intriguing. Whether such metal binding sites in human crystallins play a functional role or constitute a vestige from their evolution as lens structural proteins, remains to be elucidated.

Methods

Ethyl cyano(hydroxyimino)acetate (Oxyme pure), 9-Fluorenylmethoxycarbonyl (Fmoc) protected amino acids, and Fmoc-Rink amide MBHA resin were purchased from Merck Millipore. Propan-2-yl 1-thio- β -D-galactopyranoside (IPTG), Piperidine, N,N-dimethylformamide (DMF), 1,8-Diazabicyclo[5.4.0]undec-7-ene (DBU), N,N'-Diisopropylcarbodiimide (DIC), ethanedithiol (EDT), trifluoroacetic acid (TFA), 4-Ethylmorpholine (NEM), glycerol, and copper(II) sulfate pentahydrate ($\text{CuSO}_4 \cdot 5\text{H}_2\text{O}$) were purchased from Sigma Aldrich. HPLC grade methanol was purchased from J. T. Baker. All the aqueous solutions were prepared using ultrapure water with a resistivity $> 18 \text{ M}\Omega \text{ cm}$.

Protein expression and purification.

The pE-SUMO CRYBB2 plasmid was a gift from Larry David. The protein is expressed as a fusion protein that has a 6xHis-tagged small ubiquitin-like modifier (SUMO) at the amino-terminal extension of the β B2-crystallin. The 6xHis-tag can be removed by

digestion with Ulp1 protease, leaving the free amino group of the unmodified sequence of the protein. The plasmid pFGET19_Ulp1 was a gift from Hideo Iwai (Addgene plasmid #64697; <http://n2t.net/addgene:64697>; RRID: Addgene_64697). Ulp1 protease expression and purification was performed as previously reported. Once purified, the protease was aliquoted, dithiothreitol (DTT) and glycerol were added to a final concentration of 5mM and 25% respectively and stored at -70°C until usage.

A truncated version of βB2 -crystallin was prepared by removing the first eight amino acids from the amino-terminal region. The mutation was performed with the Q5[®] Site directed mutagenesis kit (NEB, #E0554S), using the 5'-GGCAAGCCACAGTCCC-3' forward primer and the 5'-ACCTCCAATCTGTTCGC-3' reverse primer, the truncation was confirmed by sequencing.

Both the WT and N-truncated βB2 -crystallin plasmids were transformed into E. Coli BL21-CodonPlus (DE3)-RIL chemically competent cells and expressed as follows. Briefly, a single colony from a freshly made plate was inoculated into 50 ml of Super Broth (SB) medium, enriched with ampicillin and chloramphenicol at final concentration of 50 $\mu\text{g}/\text{ml}$ each, and incubated at 37°C , 280 rpm overnight. The next day the entire culture was diluted 1:10 with SB enriched medium and incubated at the same conditions until an $\text{OD}_{600\text{nm}}$ of 2 was reached, then protein expression was induced by adding IPTG to a final concentration of 1mM and incubated for 4 hours. After protein induction, the bacteria were collected by centrifugation at $10,000 \times g$ for 5 minutes. Then the cell pellet was resuspended in lysis buffer (20 mM sodium phosphate, 300 mM NaCl, 30mM imidazole, pH=8) and 20 mg of lysozyme, were added. The bacteria were lysed first by incubation at 4°C for 30 minutes and then by 10 cycles of 30 sec of sonication at 70 % amplitude on ice. The mixture was clarified by centrifugation at $14,000 \times g$ for 45 min and then filtered through 0.45 μm pore filter.

The clarified lysate was purified by immobilized metal affinity chromatography (IMAC) using a HisTrap[™] FF 5ml column as specified by the manufacturer (Cytiva) using a ÄKTA[™] pure 25 FPLC system (Cytiva). A solution of 20 mM sodium phosphate, 500 mM NaCl, 20 mM imidazole, pH = 7.4 was used as binding/wash buffer and the same solution with 500 mM imidazole was used as elution buffer. The purification was followed by SDS-PAGE and the protein enriched fractions were mixed, concentrated by ultrafiltration (Vivaspin[™] MWCO 10 kDa, Cytiva) and buffer exchanged against binding/wash buffer using a HiPrep[™] 26/10 Desalting column (Cytiva). Then, the protein solution was digested 1:100 (v/v) with Ulp1 protease at 4°C overnight.⁶⁴ After digestion, the solution was purified again by IMAC and followed by SDS-PAGE. The enriched fractions were mixed, concentrated and buffer exchanged against Tris-HCl 30 mM, pH = 7.8 and further purified by ion exchange chromatography using a HiTrap[™] Canto[™] Q 1 ml column, with Tris-HCl 30 mM, NaCl 1M, pH = 7.8 as elution buffer. Finally, the βB2 -crystallin enriched fractions, as determined by SDS-PAGE, were mixed and buffer exchanged against MOPS 10 mM, NaCl 50mM, pH = 7.0 for non-spectroscopic studies or MOPS 20mM, NaCl 100mM, pH = 7.0 for spectroscopy experiments.

Protein purity was assured by SDS-PAGE and concentration was determined by the Lambert-Beer method using $40,910 \text{ M}^{-1}\text{cm}^{-1}$ as the molar extinction coefficient (ProtParam tool, EXPASY). The CD and EPR samples were adjusted with the appropriate volume of glycerol to a final concentration of 10 mM MOPS, 50 mM NaCl, glycerol 50 %, pH = 7.0.

Peptide synthesis and purification.

The peptide that models the N-terminal portion of the βB2 -crystallin was prepared by the solid-phase Fmoc method as previously described.²⁸ Briefly, Fmoc protected amino acids were coupled using Oxyma/DIC on DMF. Removal of the Fmoc protecting group was achieved by addition of 20% piperidine, 2% DBU in DMF and finally the peptide was cleaved by adding a mixture of 92.5% TFA, 2.5% TIS, 2.5% EDT and 2.5% H_2O . The peptide was purified by high performance liquid chromatography (HPLC) using a semi-preparative column Pursuit C18 (10 μm , 250 \times 10 mm) on a Waters HPLC system with a photodiode array (PDA) UV-vis detector. After purification the peptide was identified by mass spectrometry, lyophilized, and stored at -20°C . Peptide purity (>98%) was measured by HPLC using an analytical column Zorbax Eclipse C18 (4.5 μm , 150 \times 4.5 mm).

Turbidity assays and SDS-PAGE analysis of protein aggregates.

Turbidity assays were performed as previously described.⁴⁹ In summary, βB2 -crystallin and its N-truncated version were added to a 96-well microplate independently, and preincubated 10 minutes at 37°C and then, incubated again incubated with or without metal ions (50 μM , 200 μl final protein concentration and volume, in 10 mM MOPS, 50 mM NaCl, pH 7 buffer), then after 30 minutes of the addition of metal ions, 100 equivalents of EDTA (or an equivalent volume of buffer for non-chelating condition) were added. All samples were incubated and measured in a FluoStar Optima microplate reader. Optical dispersion was measured at 400 nm every 60 seconds during 200 minutes with a 5 s double orbital agitation period before each cycle. The experiment was performed by duplicate and each condition was measured at least by triplicate.

The protein aggregates at the endpoint of the turbidity assay were collected and separated by centrifugation into soluble and insoluble fractions. An equivalent volume of Laemmli buffer (with or without 2-mercaptoethanol) was added to each sample and boiled for 10 minutes. Each sample was loaded at room temperature into an SDS-PAGE (16%, 30:1 acrylamide/bis-acrylamide, 120 V, 90 min), after electrophoresis, the gel was stained with coomassie blue.

Titration and sample preparation.

Protein solutions were prepared at 0.3 mM concentration in 10 mM MOPS, 50 mM NaCl, 50% glycerol, pH 7 and added to a 1cm pathlength quartz spectrophotometer cell. Copper ions were added as 0.25 equivalents from a 25 mM CuSO_4 stock solution up to a 4 equivalents concentration. CD measurements were performed 5 minutes after every addition. A volume of 230–250 μl was removed from the solution at every 0.5 equivalent increment for EPR measurements. The volume of metal solution added was adjusted accordingly after taking each aliquot.

Electron Paramagnetic Resonance (EPR).

Continuous wave (CW) EPR spectra were acquired in a EMX Plus Bruker spectrometer using an X-band resonator (ER 4102ST) and a variable temperature nitrogen evaporation system (ER4131VT). The experimental parameters: microwave frequency of ~ 9.4 GHz, temperature of ~ 150 K, modulation amplitude of 5 G, microwave power of 100 mW and a modulation frequency of 100 kHz were used. Each EPR spectra represents the mean of six scans. EPR simulations were performed using the EasySpin toolbox on MATLAB.⁶⁵ A spin system of $S = \frac{1}{2}$ of Cu with natural isotopic abundance was considered. For more details see Table S1 in SI.

Circular dichroism (CD).

For copper coordination evaluation the spectra were recorded using a Jasco J-815 CD spectropolarimeter at room temperature, using a quartz cell with a 10 mm path length for copper coordination measurements. Measurements were from 280–300 to 800 nm, a bandwidth of 5 nm, every 1 nm with a scan speed of 200 nm/min and obtaining the averaged of 2 scans.

Isothermal titration calorimetry (ITC).

Experiments were performed on a VP-ITC microcalorimeter (MicroCal) at 25 °C in buffer MOPS 10 mM with NaCl 50 mM at pH 7. The protein solution (23 μ M for β B2-crystallin WT and 30 μ M for the β B2(1–6) peptide) was placed into the calorimetric cell (1.4196 mL), while the syringe (300 μ L) was filled with a CuSO_4 solution (500–750 μ M). The protein solution was filtered (200 nm) before each experiment, and the metal solution was prepared just before starting the titration. All experiments were carried out with the first titration of 1 μ L (excluded in the fitting data), followed by 29 titrations of 10 μ L. Also, at 1 and 1.5 molar ratios for β B2-crystallin WT and the β B2(1–6) peptide, respectively, unexpected signal (Figure S5) was observed (high ΔH) and for the β B2(1–6) peptide this titration was also excluded in the fitting. The solution was syringe stirred at 300 rpm. All data were fitted using the software AFFINImeter[®],⁴⁸ applying stoichiometric equilibria (ES) to each system (for a full explanation of these models please visit the website of this software: www.affinimeter.com/site/). The thermodynamic information from the best model for each system is shown in the results section. For β B2-crystallin WT a global fit of 2 independent experiments was carried out, while for β B2(1–6) peptide individual fits were performed.

Unfolding and Thermal denaturation using CD.

Measurements for unfolding were acquired in a 1 mm path length cell, from 190 to 260 nm, a bandwidth of 1 nm, every 1 nm with a scan speed of 50 nm/min and an average of two accumulations. Protein concentration was 12 μ M and was kept at room temperature in 5 mM potassium phosphate buffer solution at pH 7. For thermal denaturation experiments the protein concentration was 12 μ M and was kept in 5 mM potassium phosphate buffer solution at pH 7 in a 1mm pathlength cell. The negative signal at 215 nm was monitored between 26 °C to 90 °C with a temperature slope of 2 °C/min and a bandwidth of 1 nm. Each condition was measured by duplicate and the average data were fitted to the Gibbs-Helmholtz model for determination of the melting temperature.⁶⁶

X-Ray absorption spectroscopy (XAS).

Protein concentration was 1 mM in 10 mM MOPS, 50 mM NaCl buffer solution at pH 7. The solutions were injected into a Kapton-sealed acrylic ~140 µl sample holder of our own design, frozen in liquid nitrogen and stored until the analysis. All data were collected at SSRL beamline 15–2, which is equipped with a liquid nitrogen cooled double-crystal monochromator (Si(3,1,1)). The Cu K-alpha emission signal was detected using seven Si (444) analyzer crystals arranged in a 1m Rowland geometry and a single element silicon drift detector. The beam was focused to a beam size FWHM of 750 µm in the horizontal and 90 µm in the vertical direction. The emitted beam path was enclosed by a He-filled bag to reduce signal attenuation. To reduce photo-damage, a liquid He cooled cryostat for measurements at 10 K was used, as well as a sample stage that is equipped with motors to allow for horizontal and vertical movement for multiple sampling positions. Effects of photo-damage were carefully monitored and excluded by reducing the photon flux through beam attenuation using Al foils. Incoming energies were calibrated against the first inflection point of an internal Cu foil standard at 8978.9 eV, and the emission energies were calibrated using the elastic peaks in the emission energy range.

Prediction of Cu²⁺ binding sites.

A systematic analysis of the previously reported protein structure (PDB: 1ytq) was made. A prediction of surface exposed residues was performed using both the primary sequence (NetSurfP-2.0 online server) and the crystalline structure (PyMol).⁶⁷ Only the residues over the 25% of exposure were considered for an empirical localization of the putative coordination sites. These putative sites were compared with the ones predicted by the MIB: Metal-ion binding site prediction and docking server.⁶⁸

Supplementary Material

Refer to Web version on PubMed Central for supplementary material.

ACKNOWLEDGMENT

Authors would like to thank Patrick Frank and SSRL staff for assistance in sample preparation onsite and to A. Jessica Díaz-Salazar for technical assistance during the isothermal titration calorimetry experiments.

Funding Sources

Authors would like to thank the support from the National Council of Science and Technology (CONACYT) through grant no. PN2076, and fellowships to N.S. and M.T. Support from the Ministry of Education (SEP) through the PRODEP-CA program is also acknowledged. K. L. acknowledges funding from the National Institutes of Health, National Eye Institute (NIH R01 EY027012). N.S. is a Deutsche Forschungsgemeinschaft (DFG) International Fellow SCHU 33411/2-1. Use of the Stanford Synchrotron Radiation Lightsource and the Linac Coherent Light Source, SLAC National Accelerator Laboratory, is supported by the US Department of Energy, Office of Science, Office of Basic Energy Sciences under Contract No. DE-AC02-76SF00515. The SSRL Structural Molecular Biology Program is supported by the DOE Office of Biological and Environmental Research, and by the National Institutes of Health, National Institute of General Medical Sciences (Grant P30GM133894). O. R-M. thanks CONACyT México for a graduate student scholarship (CVU 894945). This work was supported in part by PAIP-FQ-UNAM (5000-9018) and PAPIITDGAPA-UNAM grant IN220519 to M.C.

ABBREVIATIONS

SDS-PAGE sodium dodecyl sulfate polyacrylamide gel electrophoresis

BME	2-mercaptoethanol
EPR	electron paramagnetic resonance
XAS	X-ray absorption spectroscopy
XES	X-ray emission spectroscopy
XANES	X-ray absorption near edge spectroscopy
LMCT	ligand to metal charge transfer
HγD	human γ D-crystallin protein
HγC	human γ C-crystallin protein
HγS	human γ S-crystallin protein
CD	circular dichroism
EDTA	ethylenediaminetetraacetic acid
WT	wild type protein
HAS	human serum albumin
ATCUN	amio-terminal copper and nickel binding motif
UV	ultraviolet

REFERENCES

- (1). Lam D; Rao SK; Ratra V; Liu Y; Mitchell P; King J; Tassignon MJ; Jonas J; Pang CP; Chang DF Cataract. *Nat Rev Dis Primers* 2015, 1, 15014. DOI: 10.1038/nrdp.2015.14. [PubMed: 27188414]
- (2). De Korte CL; Van Der Steen AF; Thijssen JM; Duindam JJ; Otto C; Puppels GJ Relation between local acoustic parameters and protein distribution in human and porcine eye lenses. *Exp Eye Res* 1994, 59 (5), 617–627. DOI: 10.1006/exer.1994.1147. [PubMed: 9492763]
- (3). Lovicu FJ; Lovicu FJ; Robinson ML Development of the ocular lens; Cambridge University Press, 2004.
- (4). Bloemendal H; de Jong W; Jaenicke R; Lubsen NH; Slingsby C; Tardieu A Ageing and vision: structure, stability and function of lens crystallins. *Prog Biophys Mol Biol* 2004, 86 (3), 407–485. DOI: 10.1016/j.pbiomolbio.2003.11.012. [PubMed: 15302206]
- (5). Andley UP Crystallins in the eye: Function and pathology. *Prog Retin Eye Res* 2007, 26 (1), 78–98. DOI: 10.1016/j.preteyeres.2006.10.003. [PubMed: 17166758]
- (6). Acosta-Sampson L; King J Partially folded aggregation intermediates of human gammaD-, gammaC-, and gammaS- crystallin are recognized and bound by human alphaB-crystallin chaperone. *J Mol Biol* 2010, 401 (1), 134–152. DOI: 10.1016/j.jmb.2010.05.067. [PubMed: 20621668]
- (7). Lampi KJ; Ma Z; Shih M; Shearer TR; Smith JB; Smith DL; David LL Sequence analysis of betaA3, betaB3, and betaA4 crystallins completes the identification of the major proteins in young human lens. *J Biol Chem* 1997, 272 (4), 2268–2275. DOI: 10.1074/jbc.272.4.2268. [PubMed: 8999933]
- (8). Xu J; Wang S; Zhao WJ; Xi YB; Yan YB; Yao K The congenital cataract-linked A2V mutation impairs tetramer formation and promotes aggregation of betaB2-crystallin. *PLoS One* 2012, 7 (12), e51200. DOI: 10.1371/journal.pone.0051200. [PubMed: 23236454]

- (9). Yao K; Li J; Jin C; Wang W; Zhu Y; Shentu X; Wang Q Characterization of a novel mutation in the CRYBB2 gene associated with autosomal dominant congenital posterior subcapsular cataract in a Chinese family. *Mol Vis* 2011, 17, 144–152. [PubMed: 21245961]
- (10). de Jong WW; Lubsen NH; Kraft HJ Molecular evolution of the eye lens. *Progress in Retinal and Eye Research* 1994, 13 (2), 391–442. DOI: 10.1016/1350-9462(94)90018-3.
- (11). Magabo KS; Horwitz J; Piatigorsky J; Kantorow M Expression of betaB(2)-crystallin mRNA and protein in retina, brain, and testis. *Invest Ophthalmol Vis Sci* 2000, 41 (10), 3056–3060. [PubMed: 10967064]
- (12). Piatigorsky J; DeGruyter. *Gene Sharing and Evolution : The Diversity of Protein Functions*; Harvard University Press, 2009.
- (13). Clout NJ; Kretschmar M; Jaenicke R; Slingsby C Crystal structure of the calcium-loaded spherulin 3a dimer sheds light on the evolution of the eye lens betagamma-crystallin domain fold. *Structure* 2001, 9 (2), 115–124. DOI: 10.1016/s0969-2126(01)00573-1. [PubMed: 11250196]
- (14). Kozlyuk N; Sengupta S; Bierma JC; Martin RW Calcium Binding Dramatically Stabilizes an Ancestral Crystallin Fold in Tunicate betagamma-Crystallin. *Biochemistry* 2016, 55 (50), 6961–6968. DOI: 10.1021/acs.biochem.6b00937. [PubMed: 27992995]
- (15). Shimeld SM; Purkiss AG; Dirks RPH; Bateman OA; Slingsby C; Lubsen NH Urochordate $\beta\gamma$ -Crystallin and the Evolutionary Origin of the Vertebrate Eye Lens. *Current Biology* 2005, 15 (18), 1684–1689. DOI: 10.1016/j.cub.2005.08.046. [PubMed: 16169492]
- (16). Wenk M; Baumgartner R; Holak TA; Huber R; Jaenicke R; Mayr EM The domains of protein S from *Myxococcus xanthus*: structure, stability and interactions. *J Mol Biol* 1999, 286 (5), 1533–1545. DOI: 10.1006/jmbi.1999.2582. [PubMed: 10064714]
- (17). Roskamp KW; Kozlyuk N; Sengupta S; Bierma JC; Martin RW Divalent Cations and the Divergence of betagamma-Crystallin Function. *Biochemistry* 2019, 58 (45), 4505–4518. DOI: 10.1021/acs.biochem.9b00507. [PubMed: 31647219]
- (18). Jobby MK; Sharma Y Calcium-binding to lens betaB2- and betaA3-crystallins suggests that all beta-crystallins are calcium-binding proteins. *FEBS J* 2007, 274 (16), 4135–4147. DOI: 10.1111/j.1742-4658.2007.05941.x. [PubMed: 17651443]
- (19). Aydin E; Cumurcu T; Özüğurlu F; Özyurt H; Sahinoglu S; Mendil D; Hasdemir E Levels of iron, zinc, and copper in aqueous humor, lens, and serum in nondiabetic and diabetic patients. *Biological Trace Element Research* 2005, 108 (1), 33–41. DOI: 10.1385/BTER:108:1-3:033. [PubMed: 16327057]
- (20). Balaji M; Sasikala K; Ravindran T Copper levels in human mixed, nuclear brunescence, and posterior subcapsular cataract. *British Journal of Ophthalmology* 1992, 76 (11), 668. DOI: 10.1136/bjo.76.11.668. [PubMed: 1477042]
- (21). Dawczynski J; Blum M; Winnefeld K; Strobel J Increased content of zinc and iron in human cataractous lenses. *Biol Trace Elem Res* 2002, 90 (1–3), 15–23. DOI: 10.1385/BTER:90:1-3:15. [PubMed: 12666821]
- (22). Gunduz G; Gunduz F; Yucel I; Senturk UK Levels of zinc and magnesium in senile and diabetic senile cataractous lenses. *Biol Trace Elem Res* 2003, 95 (2), 107–112. DOI: 10.1385/BTER:95:2:107. [PubMed: 14645992]
- (23). Konz I; Fernández B; Fernández ML; Pereiro R; González-Iglesias H; Coca-Prados M; Sanz-Medel A Quantitative bioimaging of trace elements in the human lens by LA-ICP-MS. *Analytical and Bioanalytical Chemistry* 2014, 406 (9), 2343–2348. DOI: 10.1007/s00216-014-7617-y. [PubMed: 24500754]
- (24). Micun Z; Falkowska M; Mlynarczyk M; Kochanowicz J; Socha K; Konopinska J Levels of Trace Elements in the Lens, Aqueous Humour, and Plasma of Cataractous Patients-A Narrative Review. *Int J Environ Res Public Health* 2022, 19 (16). DOI: 10.3390/ijerph191610376.
- (25). Srivastava VK; Varshney N; Pandey DC Role of trace elements in senile cataract. *Acta Ophthalmol (Copenh)* 1992, 70 (6), 839–841. DOI: 10.1111/j.1755-3768.1992.tb04898.x. [PubMed: 1488898]
- (26). Ciaralli L; Giordano R; Costantini S; Sepe A; Cruciani F; Moramarco A; Antonelli B; Balacco-Gabriel C Element concentrations and cataract: an experimental animal model. *J Trace Elem Med Biol* 2001, 14 (4), 205–209. DOI: 10.1016/S0946-672X(01)80003-1. [PubMed: 11396778]

- (27). Domínguez-Calva JA; Haase-Pettingell C; Serebryany E; King JA; Quintanar L A Histidine Switch for Zn-Induced Aggregation of γ -Crystallins Reveals a Metal-Bridging Mechanism That Is Relevant to Cataract Disease. *Biochemistry* 2018, 57 (33), 4959–4962. DOI: 10.1021/acs.biochem.8b00436. [PubMed: 30064223]
- (28). Quintanar L; Dominguez-Calva JA; Serebryany E; Rivillas-Acevedo L; Haase-Pettingell C; Amero C; King JA Copper and Zinc Ions Specifically Promote Nonamyloid Aggregation of the Highly Stable Human gamma-D Crystallin. *ACS Chem Biol* 2016, 11 (1), 263–272. DOI: 10.1021/acscchembio.5b00919. [PubMed: 26579725]
- (29). Ramkumar S; Fan X; Wang B; Yang S; Monnier VM Reactive cysteine residues in the oxidative dimerization and Cu(2+) induced aggregation of human gammaD-crystallin: Implications for age-related cataract. *Biochim Biophys Acta Mol Basis Dis* 2018, 1864 (11), 3595–3604. DOI: 10.1016/j.bbadis.2018.08.021. [PubMed: 30251679]
- (30). Roskamp KW; Azim S; Kassier G; Norton-Baker B; Sprague-Piercy MA; Miller RJD; Martin RW Human γ S-Crystallin–Copper Binding Helps Buffer against Aggregation Caused by Oxidative Damage. *Biochemistry* 2020, 59 (25), 2371–2385. DOI: 10.1021/acs.biochem.0c00293. [PubMed: 32510933]
- (31). Palomino-Vizcaino G; Schuth N; Domínguez-Calva JA; Rodríguez-Meza O; Martínez-Jurado E; Serebryany E; King JA; Kroll T; Costas M; Quintanar L Copper Reductase Activity and Free Radical Chemistry by Cataract-Associated Human Lens γ -Crystallins. *Journal of the American Chemical Society* 2023, 145 (12), 6781–6797. DOI: 10.1021/jacs.2c13397. [PubMed: 36918380]
- (32). Downing RS; Urbach FL Circular dichroism of square-planar, tetradentate Schiff base chelates of copper(II). *Journal of the American Chemical Society* 1969, 91 (22), 5977–5983. DOI: 10.1021/ja01050a009.
- (33). Tsangaris JM; Martin RB Visible circular dichroism of copper(II) complexes of amino acids and peptides. *Journal of the American Chemical Society* 1970, 92 (14), 4255–4260. DOI: 10.1021/ja00717a020. [PubMed: 5428384]
- (34). Fawcett TG; Bernarducci EE; Krogh-Jespersen K; Schugar HJ Charge-transfer absorptions of copper(II)-imidazole and copper(II)-imidazolate chromophores. *Journal of the American Chemical Society* 1980, 102 (8), 2598–2604. DOI: 10.1021/ja00528a013.
- (35). Daniele PG; Prenesti E; Ostacoli G Ultraviolet–circular dichroism spectra for structural analysis of copper(II) complexes with aliphatic and aromatic ligands in aqueous solution. *Journal of the Chemical Society, Dalton Transactions* 1996, (15), 3269–3275, 10.1039/DT9960003269. DOI: 10.1039/DT9960003269.
- (36). Klewpatinond M; Viles JH Empirical rules for rationalising visible circular dichroism of Cu²⁺ and Ni²⁺ histidine complexes: Applications to the prion protein. *FEBS Letters* 2007, 581 (7), 1430–1434, 10.1016/j.febslet.2007.02.068. DOI: 10.1016/j.febslet.2007.02.068 (accessed 2023/02/09). [PubMed: 17359979]
- (37). Stanyon HF; Cong X; Chen Y; Shahidullah N; Rossetti G; Dreyer J; Papamokos G; Carloni P; Viles JH Developing predictive rules for coordination geometry from visible circular dichroism of copper(II) and nickel(II) ions in histidine and amide main-chain complexes. *The FEBS Journal* 2014, 281 (17), 3945–3954, 10.1111/febs.12934. DOI: 10.1111/febs.12934 (accessed 2023/02/09). [PubMed: 25039600]
- (38). Bal W; Christodoulou J; Sadler PJ; Tucker A Multi-metal binding site of serum albumin. *Journal of Inorganic Biochemistry* 1998, 70 (1), 33–39. DOI: 10.1016/S0162-0134(98)00010-5. [PubMed: 9661286]
- (39). Sankararamakrishnan R; Verma S; Kumar S ATCUN-like metal-binding motifs in proteins: Identification and characterization by crystal structure and sequence analysis. *Proteins: Structure, Function, and Bioinformatics* 2005, 58 (1), 211–221, 10.1002/prot.20265. DOI: 10.1002/prot.20265 (accessed 2023/02/09).
- (40). Neupane KP; Aldous AR; Kritzer JA Metal-binding and redox properties of substituted linear and cyclic ATCUN motifs. *Journal of Inorganic Biochemistry* 2014, 139, 65–76. DOI: 10.1016/j.jinorgbio.2014.06.004. [PubMed: 24980953]
- (41). Gonzalez P; Bossak K; Stefaniak E; Hureau C; Raibaut L; Bal W; Faller P N-Terminal Cu-Binding Motifs (Xxx-Zzz-His, Xxx-His) and Their Derivatives: Chemistry, Biology and

- Medicinal Applications. *Chemistry – A European Journal* 2018, 24 (32), 8029–8041, 10.1002/chem.201705398. DOI: 10.1002/chem.201705398 (accessed 2023/02/09). [PubMed: 29336493]
- (42). Harford C; Sarkar B Amino Terminal Cu(II)- and Ni(II)-Binding (ATCUN) Motif of Proteins and Peptides: Metal Binding, DNA Cleavage, and Other Properties. *Accounts of Chemical Research* 1997, 30 (3), 123–130. DOI: 10.1021/ar9501535.
- (43). Schwab S; Shearer J; Conklin SE; Alios B; Haas KL Sequence proximity between Cu(II) and Cu(I) binding sites of human copper transporter 1 model peptides defines reactivity with ascorbate and O₂. *Journal of Inorganic Biochemistry* 2016, 158, 70–76. DOI: 10.1016/j.jinorgbio.2015.12.021. [PubMed: 26778425]
- (44). Bossak K; Drew SC; Stefaniak E; Płonka D; Bonna A; Bal W The Cu(II) affinity of the N-terminus of human copper transporter CTR1: Comparison of human and mouse sequences. *Journal of Inorganic Biochemistry* 2018, 182, 230–237. DOI: 10.1016/j.jinorgbio.2018.01.011. [PubMed: 29402466]
- (45). Stefaniak E; Płonka D; Drew SC; Bossak-Ahmad K; Haas KL; Pushie MJ; Faller P; Wezynfeld NE; Bal W The N-terminal 14-mer model peptide of human Ctr1 can collect Cu(ii) from albumin. Implications for copper uptake by Ctr1†. *Metallomics* 2018, 10 (12), 1723–1727. DOI: 10.1039/c8mt00274f (accessed 2/9/2023). [PubMed: 30489586]
- (46). Bossak-Ahmad K; Fr czyk T; Bal W; Drew SC The Sub-picomolar Cu₂₊ Dissociation Constant of Human Serum Albumin. *ChemBioChem* 2020, 21 (3), 331–334, 10.1002/cbic.201900435. DOI: 10.1002/cbic.201900435 (accessed 2023/02/09). [PubMed: 31298451]
- (47). Wezynfeld NE; Vileno B; Faller P Cu(II) Binding to the N-Terminal Model Peptide of the Human Ctr2 Transporter at Lysosomal and Extracellular pH. *Inorganic Chemistry* 2019, 58 (11), 7488–7498. DOI: 10.1021/acs.inorgchem.9b00711. [PubMed: 31083932]
- (48). Piñeiro Á; Muñoz E; Sabín J; Costas M; Bastos M; Velázquez-Campoy A; Garrido PF; Dumas P; Ennifar E; García-Río L; Rial J; Pérez D; Fraga P; Rodríguez A; Coteló C AFFINImeter: A software to analyze molecular recognition processes from experimental data. *Analytical Biochemistry* 2019, 577, 117–134. DOI: 10.1016/j.ab.2019.02.031. [PubMed: 30849378]
- (49). Palomino-Vizcaino G; Domínguez-Calva JA; Schuth N; Martínez-Jurado E; Rodríguez-Meza O; Serebryany E; King JA; Kroll T; Costas M; Quintanar L 2023. DOI: 10.26434/chemrxiv-2022-3k5d5.
- (50). Kau LS; Spira-Solomon DJ; Penner-Hahn JE; Hodgson KO; Solomon EI X-ray absorption edge determination of the oxidation state and coordination number of copper. Application to the type 3 site in *Rhus vernicifera* laccase and its reaction with oxygen. *Journal of the American Chemical Society* 1987, 109 (21), 6433–6442. DOI: 10.1021/ja00255a032.
- (51). Zhang K; Zhao W-J; Leng X-Y; Wang S; Yao K; Yan Y-B The importance of the last strand at the C-terminus in β B2-crystallin stability and assembly. *Biochimica et Biophysica Acta (BBA) - Molecular Basis of Disease* 2014, 1842 (1), 44–55. DOI: 10.1016/j.bbadis.2013.10.001. [PubMed: 24120835]
- (52). Dominguez-Calva JA; Perez-Vazquez ML; Serebryany E; King JA; Quintanar L Mercury-induced aggregation of human lens gamma-crystallins reveals a potential role in cataract disease. *J Biol Inorg Chem* 2018, 23 (7), 1105–1118. DOI: 10.1007/s00775-018-1607-z. [PubMed: 30167892]
- (53). Pettit LD; Pyburn S; Bal W; Kozłowski H; Bataille M A study of the comparative donor properties to Cu of the terminal amino and imidazole nitrogens in peptides. *Journal of the Chemical Society, Dalton Transactions* 1990, (12), 3565–3570, 10.1039/DT9900003565. DOI: 10.1039/DT9900003565.
- (54). Mital M; Wezynfeld NE; Fraczyk T; Wiloch MZ; Wawrzyniak UE; Bonna A; Tumpach C; Barnham KJ; Haigh CL; Bal W; Drew SC A Functional Role for Abeta in Metal Homeostasis? N-Truncation and High-Affinity Copper Binding. *Angew Chem Int Ed Engl* 2015, 54 (36), 10460–10464. DOI: 10.1002/anie.201502644. [PubMed: 26178596]
- (55). Miesbauer LR; Smith JB; Smith DL Amino acid sequence of human lens beta B2-crystallin. *Protein Sci* 1993, 2 (2), 290–291. DOI: 10.1002/pro.5560020217. [PubMed: 8443605]
- (56). Lampi KJ; Oxford JT; Bachinger HP; Shearer TR; David LL; Kapfer DM Deamidation of Human β B1 Alters the Elongated Structure of the Dimer. *Experimental Eye Research* 2001, 72 (3), 279–288. DOI: 10.1006/exer.2000.0950. [PubMed: 11180977]

- (57). Kim YH; Kapfer DM; Boekhorst J; Lubsen NH; Bächinger HP; Shearer TR; David LL; Feix JB; Lampi KJ Deamidation, but Not Truncation, Decreases the Urea Stability of a Lens Structural Protein, β B1-Crystallin. *Biochemistry* 2002, 41 (47), 14076–14084. DOI: 10.1021/bi026288h. [PubMed: 12437365]
- (58). Lampi KJ; Kim YH; Bachinger HP; Boswell BA; Lindner RA; Carver JA; Shearer TR; David LL; Kapfer DM Decreased heat stability and increased chaperone requirement of modified human betaB1-crystallins. *Mol Vis* 2002, 8, 359–366. [PubMed: 12355063]
- (59). Lampi KJ; Amyx KK; Ahmann P; Steel EA Deamidation in Human Lens β B2-Crystallin Destabilizes the Dimer. *Biochemistry* 2006, 45 (10), 3146–3153. DOI: 10.1021/bi052051k. [PubMed: 16519509]
- (60). Werten PJJ; Lindner RA; Carver JA; de Jong WW Formation of β A3/ β B2-crystallin mixed complexes: involvement of N- and C-terminal extensions. *Biochimica et Biophysica Acta (BBA) - Protein Structure and Molecular Enzymology* 1999, 1432 (2), 286–292. DOI: 10.1016/S0167-4838(99)00123-5. [PubMed: 10407150]
- (61). Shih M; Lampi KJ; Shearer TR; David LL Cleavage of beta crystallins during maturation of bovine lens. *Mol Vis* 1998, 4, 4. [PubMed: 9485487]
- (62). Robertson LJG; David LL; Riviere MA; Wilmarth PA; Muir MS; Morton JD Susceptibility of Ovine Lens Crystallins to Proteolytic Cleavage during Formation of Hereditary Cataract. *Investigative Ophthalmology & Visual Science* 2008, 49 (3), 1016–1022. DOI: 10.1167/iov.07-0792 (accessed 5/11/2023). [PubMed: 18326725]
- (63). Srivastava OP; Srivastava K β B2-crystallin undergoes extensive truncation during aging in human lenses. *Biochemical and Biophysical Research Communications* 2003, 301 (1), 44–49. DOI: 10.1016/S0006-291X(02)02975-3. [PubMed: 12535638]
- (64). Guerrero F; Ciragan A; Iwai H Tandem SUMO fusion vectors for improving soluble protein expression and purification. *Protein Expression and Purification* 2015, 116, 42–49. DOI: 10.1016/j.pep.2015.08.019. [PubMed: 26297996]
- (65). Stoll S; Schweiger A EasySpin, a comprehensive software package for spectral simulation and analysis in EPR. *Journal of Magnetic Resonance* 2006, 178 (1), 42–55. DOI: 10.1016/j.jmr.2005.08.013. [PubMed: 16188474]
- (66). Greenfield NJ Using circular dichroism collected as a function of temperature to determine the thermodynamics of protein unfolding and binding interactions. *Nature Protocols* 2006, 1 (6), 2527–2535. DOI: 10.1038/nprot.2006.204. [PubMed: 17406506]
- (67). Klausen MS; Jespersen MC; Nielsen H; Jensen KK; Jurtz VI; Sønderby CK; Sommer MOA; Winther O; Nielsen M; Petersen B; Marcatili P NetSurfP-2.0: Improved prediction of protein structural features by integrated deep learning. *Proteins: Structure, Function, and Bioinformatics* 2019, 87 (6), 520–527, 10.1002/prot.25674. DOI: <https://doi.org/10.1002/prot.25674> (accessed 2023/02/09).
- (68). Lin Y-F; Cheng C-W; Shih C-S; Hwang J-K; Yu C-S; Lu C-H MIB: Metal Ion-Binding Site Prediction and Docking Server. *Journal of Chemical Information and Modeling* 2016, 56 (12), 2287–2291. DOI: 10.1021/acs.jcim.6b00407. [PubMed: 27976886]

Synopsis

The β B2-crystallin interaction with copper is a very complex process. It leads to protein aggregation by several mechanisms. This protein has several binding sites, which are revealed by spectroscopic studies. One of them is an N-terminal ACTUN-like with nanomolar affinity for copper, and it may have a physiologically relevant protecting role against copper-induced aggregation.

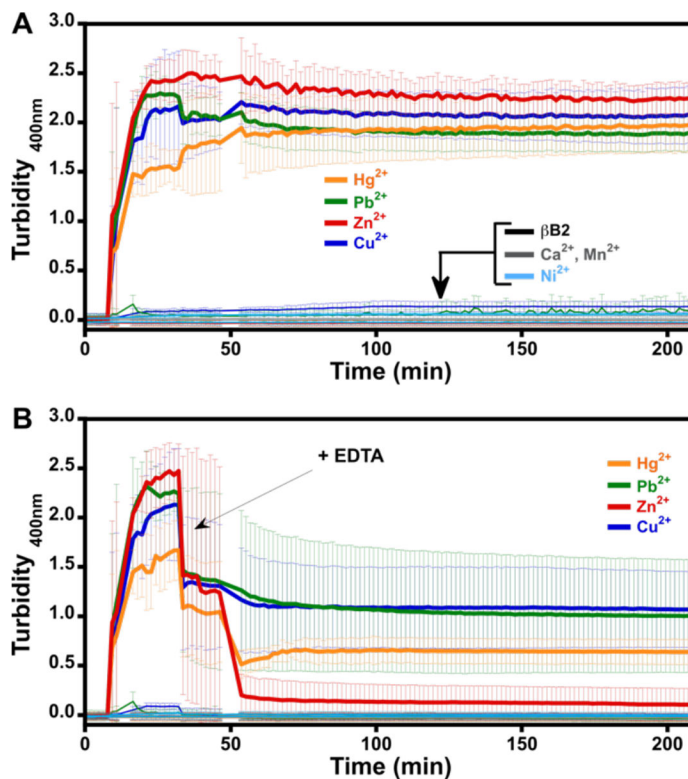


Figure 1.

Metal induced aggregation of β B2-crystallin. Turbidity assays of β B2-crystallin 50 μ M with 10 equivalents of different metal ions: Mn^{2+} , Ca^{2+} , Ni^{2+} (black traces near the baseline), Hg^{2+} (yellow trace), Pb^{2+} (green trace), Zn^{2+} (red trace), and Cu^{2+} (blue trace) (A); and the impact of ethylenediaminetetraacetic acid (EDTA) (B). Metal ions were added after 10 min of incubation of the protein at 37 $^{\circ}\text{C}$. The arrow indicates the addition of 100 equivalent of EDTA, 30 min after addition of the metal ion (i.e. at total time=40 min); a small change in baseline can be observed at 40 min in A, due to the addition of 20 μ l of MOPS buffer. Average turbidity of six replicate assays with the corresponding standard deviations is plotted.

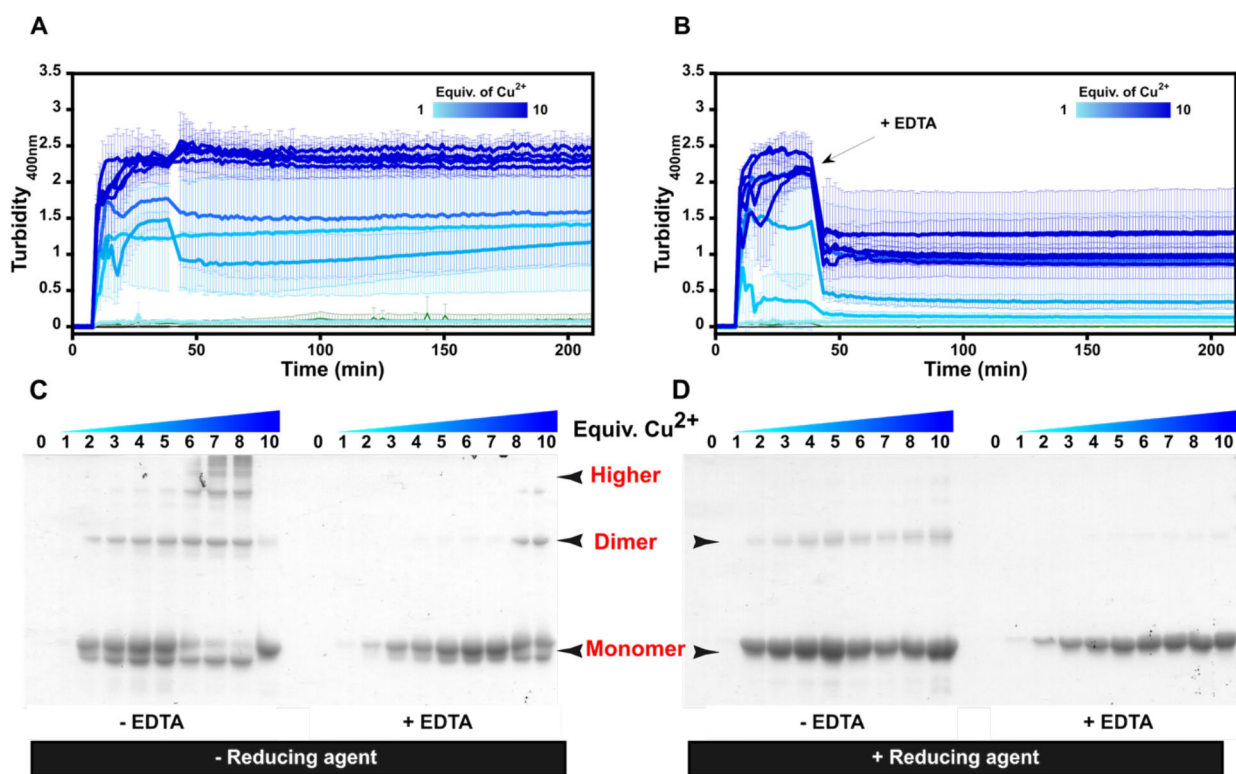


Figure 2.

Copper induced aggregation of β B2-crystallin. Turbidity assays of β B2-crystallin ($50\mu\text{M}$) with increasing number of equivalents of Cu^{2+} ions (**A**); and the impact of ethylenediaminetetraacetic acid (EDTA) (**B**). Cu^{2+} ions were added after 5 minutes of incubation of the protein at 37°C . The arrow indicates the addition of 100 equiv. of EDTA, 30 min after copper addition. SDS-PAGE analysis of the protein aggregates ($4\mu\text{g}$) at the endpoint of the turbidity assays, with (**C**) and without (**D**) 2-mercaptoethanol (BME) as reducing agent. Average turbidity of four replicate assays with the corresponding standard deviations is plotted.

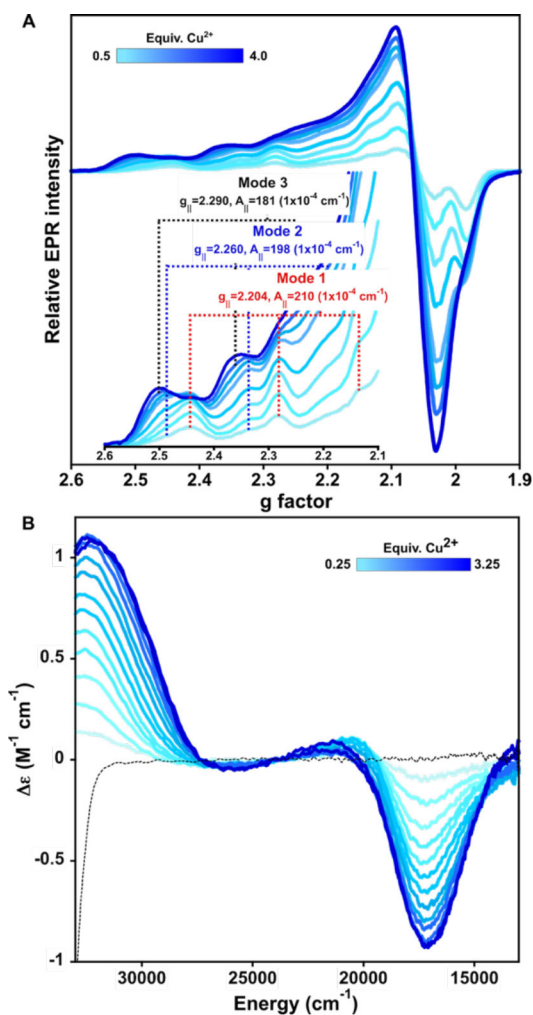


Figure 3. Copper coordination to β B2-crystallin. Titration of β B2-crystallin 0.3 mM by Cu^{2+} (0 to 3.5 equiv) as followed by electron paramagnetic resonance (EPR) (A) and circular dichroism (CD) (B). Each spectrum represents the incremental addition of 0.25 (for CD) or 0.5 (for EPR) equiv. (light to dark blue traces). Parallel region of the EPR spectra is shown in the inset of (A).

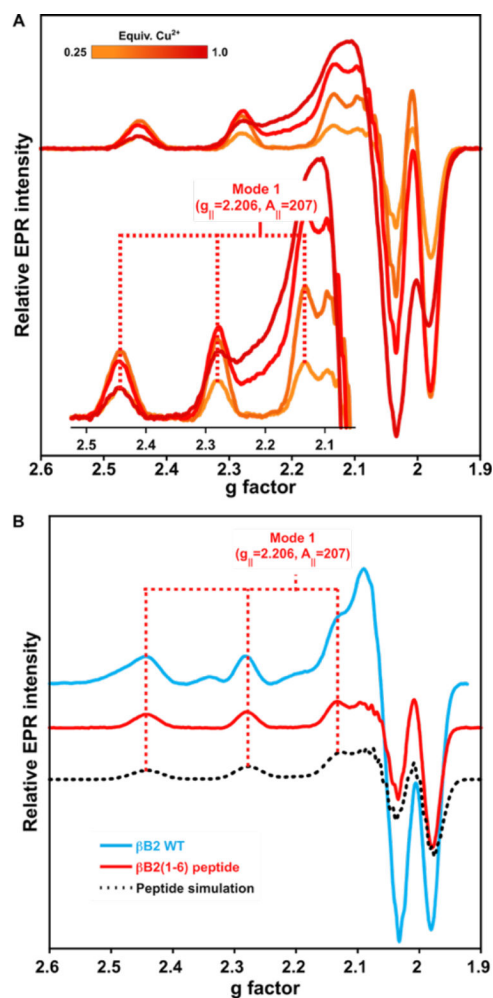


Figure 4. Copper coordination to β B2(1–6) peptide. **A)** Titration of the peptide ASDHQP (0.3 mM) by Cu^{2+} ions (0.25, 0.5, 0.75 & 1equiv) as followed by EPR. The inset shows the parallel hyperfine region indicating the copper coordination parameters. **B)** EPR spectra comparison of the β B2 WT protein (with 1 equiv. Cu^{2+}), the β B2(1–6) peptide (with 0.5 equiv. Cu^{2+}). EPR simulations are shown in dotted lines, using parameters listed in Table S1.

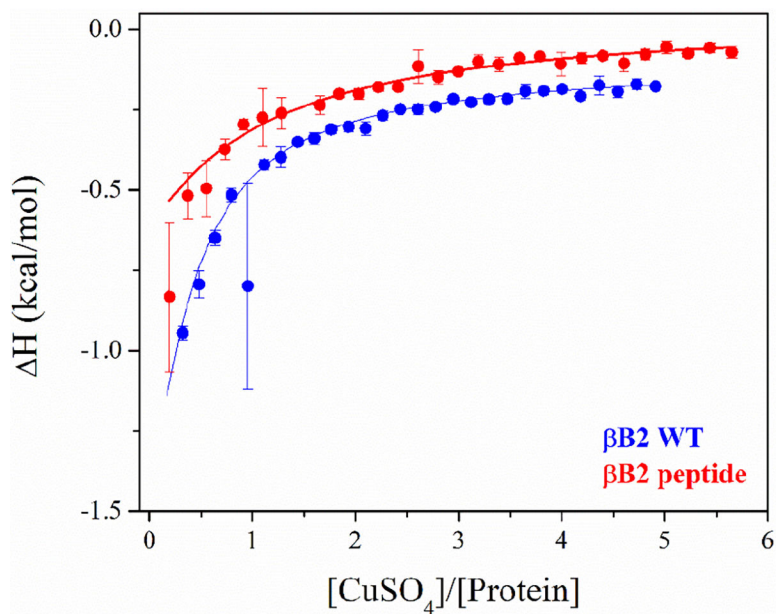


Figure 5.

ITC experiments of $\beta\text{B2 WT}$ (blue) and $\beta\text{B2 peptide}$ (red) with copper at 25 °C. Data were obtained from 30 titrations of 10 μL of CuSO_4 (500–750 μM) into a fresh protein solution (23 μM for $\beta\text{B2 WT}$ and 30 μM for $\beta\text{B2 peptide}$) in 10mM MOPS buffer, pH 7.0. Raw ITC data are shown in Figure S6. ITC data were fitted using the software AFFINImeter,⁴⁸ and the best model was selected based on the lowest value of χ^2 .

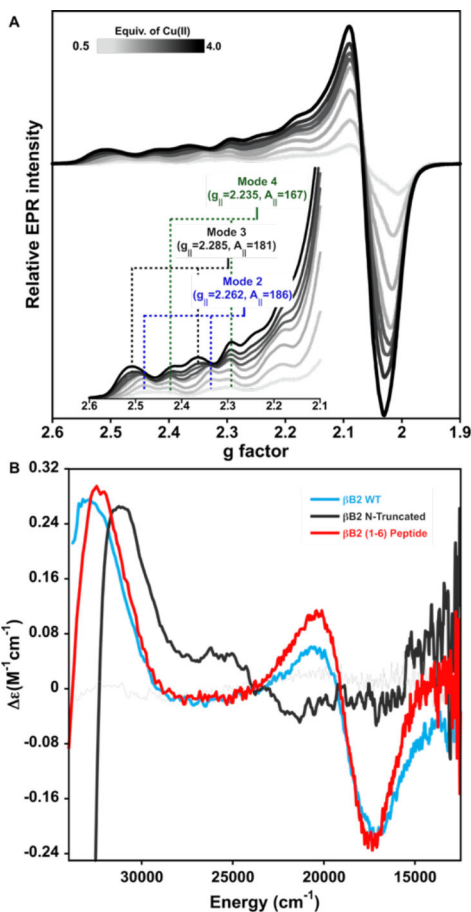


Figure 6. Copper coordination to N-truncated β B2-crystallin. (A) Titration of N-truncated β B2-crystallin protein 0.3 mM by Cu^{2+} ions as followed by EPR. Each spectrum represents the addition of incremental 0.5 equiv (light to dark gray traces) of the metal ion. Parallel region of the EPR spectra is shown in the inset of (A). (B) Comparison of the CD spectra of β B2-crystallin WT with 1 equiv. of Cu^{2+} (blue trace), the β B2(1–6) peptide with 0.5 equiv. of Cu^{2+} (red trace) and N-truncated protein with 1 equiv. of Cu^{2+} (gray trace).

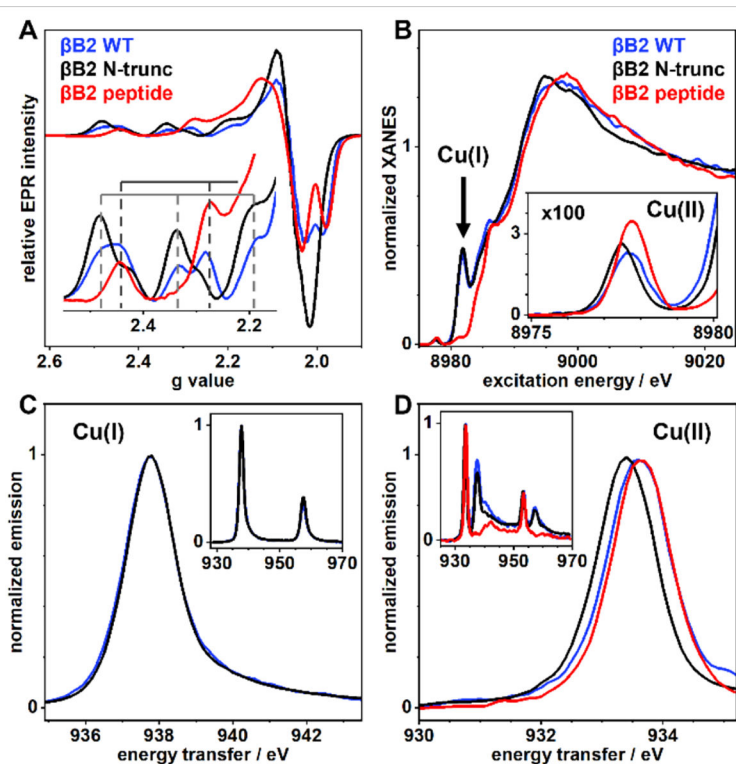


Figure 7.

Spectroscopic comparison of copper bound to β B2-crystallin WT (blue trace), the β B2(1–6) peptide (red trace) and N-truncated protein (gray trace) by EPR (A), XANES (B) and XES (C&D). Protein/peptide concentrations were 1 mM and 1 equiv of Cu^{2+} ions were added. The inset in A shows the parallel region of the EPR spectra. The inset in B shows a magnification of the Cu^{2+} pre-edge features in the 8975–8980 eV region. Normalized XES in C & D correspond to $2p^{3/2} \rightarrow 1s$ transitions ($K\alpha$ emission) after resonant excitation of Cu^+ (C) or Cu^{2+} (D) specific K-edge absorption; the inset shows both $2p \rightarrow 1s$ transitions. Energy axes correspond to the energy difference between emission and absorption to account for different excitation energies. Excitation energies in C are 8981.81 eV for β B2 WT and β B2 N-trunc, and 8977.61 eV (β B2 WT), 8977.43 eV (β B2 N-trunc), and 8977.68 eV (β B2 peptide) in D.

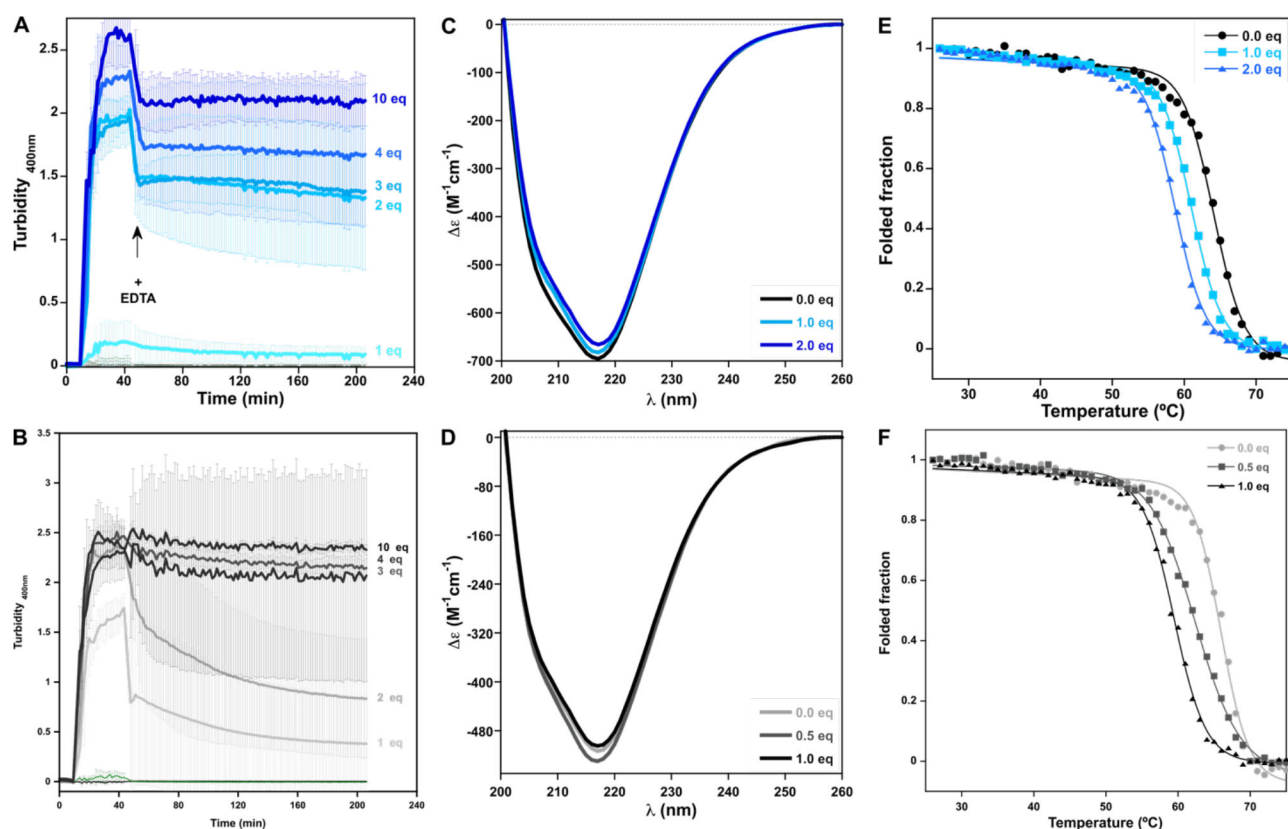


Figure 8.

Comparison of the impact of Cu²⁺ ions in the aggregation (A & B; each trace represents the average of three repetitions and the standard deviation is represented as error bars), folding (C & D) and thermal stability (E & F; each trace represents the average of two independent repetitions) of βB2-crystallin WT (A, C & E) and the N-truncated protein (B, D & F). Turbidity assays of βB2-crystallin WT (A) and the N-truncated protein (B) 50 μM with increasing number of equivalents of Cu²⁺ ions, and the impact of ethylenediaminetetraacetic acid (EDTA); Cu²⁺ ions were added after 5 minutes of incubation of the protein at 37 °C; the arrow indicates the addition of 100 equiv. of EDTA, 30 min after copper addition. Average turbidity of four replicate assays with the corresponding standard deviations are plotted. Titration of βB2-crystallin WT (C) and the N-truncated protein (D) 12 μM with Cu²⁺ ions, as followed by near UV CD. Thermal denaturation assays of βB2-crystallin WT (E) and the N-truncated protein (F) 12 μM with different amounts of Cu²⁺ ions; solid lines correspond to fitting curves. The extracted thermodynamic parameters are listed in Table S2. Individual thermal denaturation traces (Fig. S13A and B) are reported in SI.

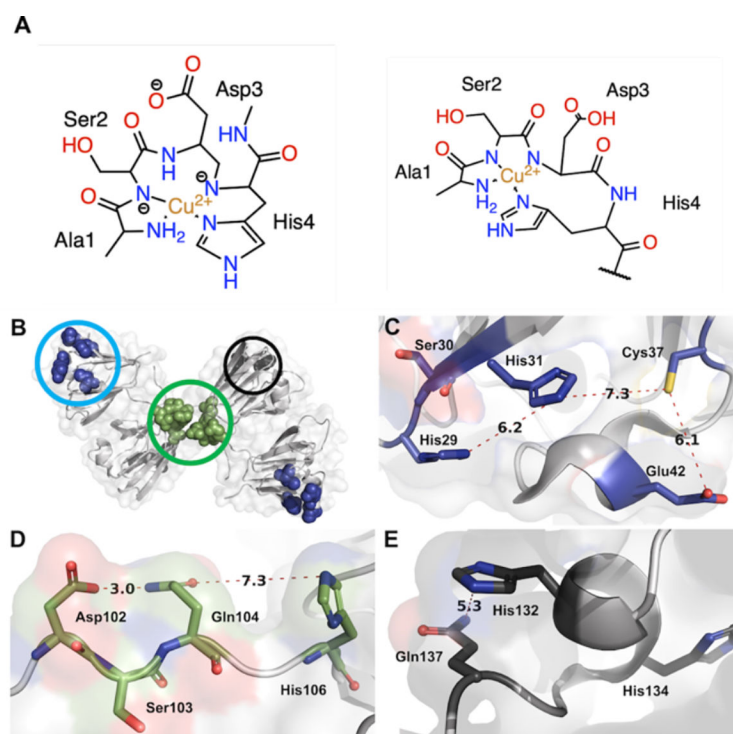


Figure 9. Putative copper binding sites in β B2-crystallin. A) Proposed structures for the Cu^{2+} -ATCUN-like complex of β B2-crystallin. B) Cartoon representation of the domain swapped protein dimer (PDB: 1YTQ) with three putative binding sites highlighted: C) A putative coordination site at the N-terminal globular domain; D) A potential binding site at the dimer interface involving the polypeptide that connects the globular domains; and E) A putative coordination site at the C-terminal domain. The residues involved and distances between them are shown in angstroms.

Table 1.

Thermodynamic parameters for interaction of β B2 WT and β B2 peptide with copper. Data were obtained from the fitting of ITC data using the software AFFINImeter.

	Model (protein metal)	K_A (M^{-1})	K_d (nM)	H (kcal/mol)
<i>βB2 WT protein</i>	2:1	$1.11 \pm 0.05 \times 10^9$	0.9	-3.12 ± 0.05
<i>βB2 peptide</i>	2:1	$1.17 \pm 0.11 \times 10^8$	8.5	-6.11 ± 0.31